OPTIMIZATION OF AXIAL FANS WITH HIGHLY SWEPT BLADES WITH RESPECT TO LOSSES AND NOISE REDUCTION

Konrad BAMBERGER, Thomas CAROLUS

University of Siegen, Paul-Bonatz-Strasse 9-11,
57223 Siegen, Germany

SUMMARY

A low pressure axial fan with swept blades was optimized with respect to sound emission and efficiency. Noise is addressed by a modified sweep strategy. Regarding aerodynamics, geometrical parameters describing variations of the blade profile and hub contour were defined. The optimum in terms of maximal total-to-total fan efficiency at the design point was approached by numerous CFD simulations embedded in the Nelder-Mead optimization method. Besides a moderate increase in efficiency at the design point, a remarkable extension of operating range was observed. The numerical results were successfully validated. Acoustic measurements furthermore showed a decrease in sound emission over the complete operating range.

NOMENCLATURE

Latin symbols

A	surface area
c	absolute velocity
d	thickness (of airfoil)
D	fan diameter
f	maximal camber of airfoil
l	length (e.g. chord length)
L	sound level
n	rotational speed
p	pressure
P	shaft power
r	radius
$\dot{V}$	volume flow rate
w	relative velocity
x	streamwise coordinate of airfoils
z	axial coordinate of fan

Greek symbols

η	efficiency
θ	angle around rotational axis
λ	sweep angle
ν	hub-to-tip ratio
ρ	density
ϕ	flow coefficient
ψ	pressure rise coefficient

Subscripts and indices

ax	axial
f	camber
h	hub
m	midspan
p	(sound) pressure
s	shroud
t	total
ts	total-to-static
tt	total-to-total
W	(sound) power

Abbreviations

CFD	Computational Fluid Dynamics
LE	leading edge
RANS	Reynolds-averaged-Navier-Stokes
SL	stacking line
SST	shear stress transport
TE	trailing edge

INTRODUCTION

The main objectives in axial fan design are high efficiency and low sound emission over a wide operating range. A successful design strategy with respect to noise is blade sweep. In our terms a swept blade is inclined by a sweep angle λ between the vector-mean relative flow direction from into outlet and the blade leading edge (LE), trailing edge (TE) or stacking line (SL). This is in contrast to a “skewed” blade, where blade elements a merely shifted in circumferential direction. Figure 1 illustrates the definition of the sweep angle in a 3D and 2D sketch. The example shows a blade without dihedral but constant sweep angle. In general, λ is variable over the blade radius. The convention is that positive values of λ refer to sweep in circumferential direction ("forward sweep") and negative values of λ refer to sweep against the circumferential direction ("backward sweep"). A detailed description is given by Beiler [1].

A discussion of the effect of blade sweep on the known noise mechanisms in fans is amongst others presented by Wright [2] and Carolus [3]. One effective noise source is the interaction of the rotating blades with the incoming small-scale turbulence which results in unsteady blade forces. This mechanism of noise generation is concentrated at the front part of the profile and can thus be alleviated by sweeping the leading edge. A swept leading edge contributes to phase-shift canceling of noise generated at different spanwise positions. Fundamental work on this effect was done by Kerschen [4] who investigated single blades with high-frequency gusts in the inflow and proved a strong coherence between sweep angle and sound emission. Other noise sources are the turbulent boundary layer and its interaction with the trailing edge. Ffowcs Williams and Hall [5] discovered that the presence of a scattering half plane in a turbulent fluid largely increases the noise generated and that the intensity is dependent on the angle between the flow and the plane (the trailing edge sweep angle). Numerous further investigations consider the impact of sweep on self noise or the difference

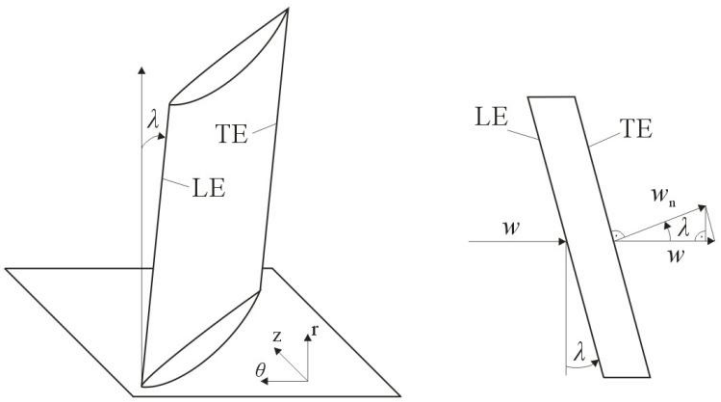

Figure 1: Schematic of a swept blade indicating the sweep angle λ and the relative velocity w.

between backward and forward sweep which is however not relevant for this work.

The other objective of this work - the enhancement of efficiency - leads to the analysis of secondary flows. The focus is on near-wall flows at the blade and hub. A general phenomenon in turbomachinery is the radial flow in low-momentum regions (the boundary layers) due to centrifugal forces. This can partly be suppressed by forward swept blades where the curving path of the centrifuged boundary layer fluid is truncated resulting in both, aerodynamic and aeroacoustic advantages [2]. However, the extent of forward sweep is often limited by packaging and strength considerations. To which extent radial flow can be considered in the design depends on the design method selected. Carolus [6] describes a quasi 2D design method based on the blade element theory. Radial flow is accounted for by consideration of the radial equilibrium on a fluid element. The weakness of this method is that it assumes rotational symmetry which is never the case. Moreover, pressure and velocities are only considered in planes upstream and downstream of the rotor while local effects are neglected. It is sufficient to know the polar curve of the selected airfoil profile for each blade element, i.e. the lift and drag coefficients over the angle of attack. The streamwise pressure distribution on a blade element is not important for this design method. However, since the streamwise pressure distribution is never constant over the span (especially for swept blades), there always occurs a radial pressure gradient either enforcing or alleviating the local radial flow. The extent of the gradient depends among others on the local curvature of the profile. The streamwise pressure distribution on a profile can be computed by 2D methods. Much of the theory is presented by Abbot in the book "Theory of Wing Sections" [7]. Profiles selected primarily to reduce secondary flows might differ from those with promising 2D polar curves and it is extremely difficult to predict the impact on efficiency and to find an aerodynamic optimum. 3D inverse design methods as presented by Zangeneh [8] are more precise in the prediction of three dimensional flows and have already been coupled with optimization methods. Nevertheless, only simulations by means of Computational Fluid Dynamics (CFD) provide full 3D solutions of the complete viscid flow field. Especially the complex system of secondary flows at the tip clearance and in the hub area is only partly covered by the inverse design method. A model of secondary flows near the hub is presented by Takeishi [9] (see Figure 2). Although most losses occur in the passage vortex, specific measures to reduce losses often focus on the crossflow "B" which is driven by the circumferential pressure gradient from each blade's pressure side to the suction side of the adjacent blade. Eliminating or reducing this crossflow is assumed to delay the generation of the passage vortex. The idea to reduce the pressure gradient by a non-axisymmetric endwall with a convex contour adjacent each blade pressure side and a concave contour adjacent each blade suction side was patented by Rolls-Royce [10]. Axisymmetric endwall contouring has been applied successfully as well. Axisymmetric endwall contouring is

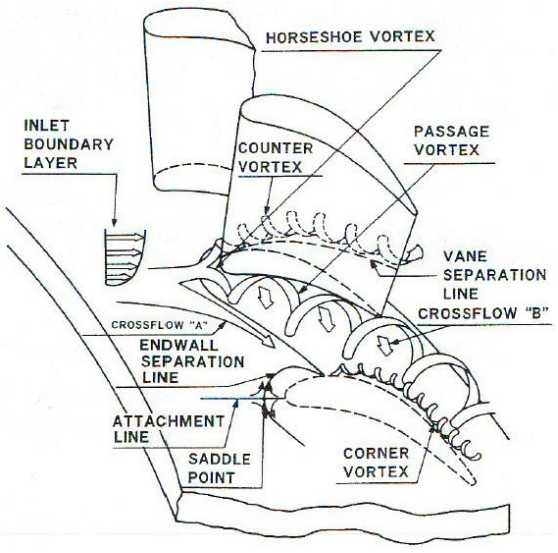

Figure 2: Endwall secondary flow model after Takeishi [9].

much less effective in changing the circumferential pressure gradient as compared to non-axisymmetric contouring and is mainly used to condition the streamwise pressure gradient. The remaining effect regarding the circumferential pressure gradient is that equal curvature at two different circumferential locations still has a different influence on pressure if the velocity or boundary layer thickness is different. Recent work on axisymmetric contouring was done by the German Aerospace Centre [11] who increased the efficiency of a gas turbine compressor stage by a wavy casing. An evolutionary optimization algorithm was used and the target functions were solved by a CFD code. While numerous investigations regarding endwall contouring in high pressure compressors have been conducted and much literature on that is available, there is only very little experience about its application in low pressure fans.

It is a very demanding task to analytically design a fan with reduced secondary flow or to draw the right conclusions from a single CFD simulation. In general, the design process will cover a set of iterations with adapted designs and repeated simulations which are ideally embedded in an optimization algorithm. Thévenin [12] recently published a book on CFD based optimization which mainly refers to simplex, evolutionary or adjoint methods. Simplex methods are easiest to implement. This method was developed by Nelder and Mead (referred to as the Nelder-Mead method) [13]. It is based on comparison of function values at the $(N+1)$ vertices of a general simplex, N being the number of optimization parameters. The vertex with the worst value is replaced continuously by other points. One weakness is that the optimum approached can be local. On top of that, this method is limited to a single target function. Evolutionary algorithms allow for several target functions and are less at risk to converge to local optima. The disadvantage is increased initialization effort (the first generation) meaning that the performance does not improve straight away. Adjoint methods require specific CFD codes that are not yet commercially available.

METHODOLOGY

General design strategy

The design target of reduced shaft power required and lower sound emission as compared to a benchmark fan is approached by sequential steps. New considerations in terms of sweep lead to a modified design philosophy which was then used to design the first rotor. Beginning with this design, the blade profile was optimized aerodynamically by the aid of CFD simulations. Given the optimized blade geometry, an axisymmetric endwall contour was applied and optimized as well. Finally, the latest design was validated and acoustic measurements were conducted for both fans.

Benchmark fan

The benchmark fan was designed at the University of Siegen based on a quasi 2D blade element method [6]. Its main characteristics are summarized in Table 1. The flow and pressure rise coefficient are defined as usual:

$$\phi = \frac{\dot{V}}{\frac{\pi^2}{4} D^3 n} \tag{1}$$

$$\psi = \frac{\Delta p}{\frac{\pi^2}{2} D^2 n^2 \rho} \tag{2}$$

Table 1: Characteristics of the benchmark fan.

Shroud diameter	D	0.3 m
Rotational speed	n	41.67 s^{-1} (2500 min^{-1})
Hub-to-tip ratio	ν	0.5
Flow coefficient at design point	φ	0.222
Total to static pressure rise coefficient at design point	ψ_{ts}	0.171

Sweep strategy

In the first step of the design the sweep angle is specified as the angle between the stacking line that typically goes through the centre of gravity of the blades element, and a radial beam. However, the actual sweep at leading and trailing edge are also affected by spanwise variations in chord length. Variable chord lengths are typical when the load distribution is predefined and also occurs in the benchmark fan.
Figure 3 shows schematics of untwisted blades with constant and variable chord length. It is obvious that - in case of the variable chord length design - the sweep angle of LE and TE can deviate from the sweep of the stacking line and hence the noise reduction anticipated by LE and TE sweep. Therefore, the design strategy reported here uses constant chord length from hub to tip to avoid the undesired sweep deviations described above. The chord length is adjusted such that the fan meets the design point. This means moving away from a predefined aerodynamic load distribution.

Geometrical parameters of the blade profile

Four digit NACA profiles were used throughout the optimization process. These profiles are described by three parameters that are usually normalized with the chord length l:

- Maximum camber: f/l
- Position of max. camber: x_f/l
- Maximum Thickness: d/l

A decision was taken to exclude the thickness from the optimization process. It is determined from structural considerations and decays linearly from d/l = 11% at hub to d/l = 9% at tip. The spanwise distributions of f/l and x_f/l were assumed to follow quadratic functions that meet specified values at hub, shroud and midspan. Consequently, the optimization problem was to find the optimal values of f/l and x_f/l at those three positions. In contrast to the former design strategy, "optimal" no longer means the lowest ratio of drag to lift at isolated blade elements, but the lowest overall loss taking all 3D effects into account.

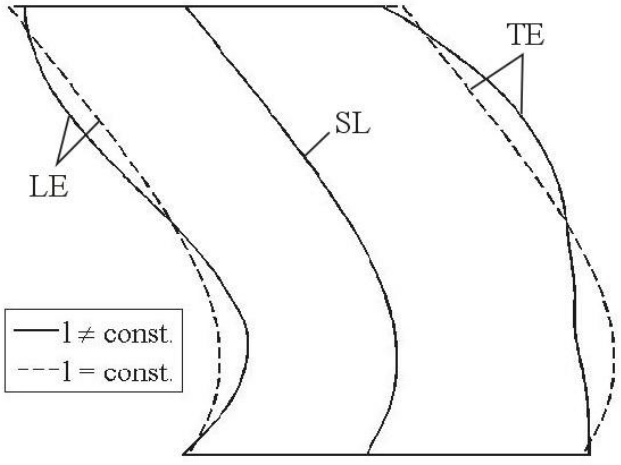

Figure 3: Untwisted blade: Impact of variable chord length on LE/TE sweep.

Geometrical parameters of the hub contour

The hub contour is described by the function $r_h^*=(r_{h,0}+\Delta r(z^*))/r_{h,0}$ where $r_{h,0}$ is the hub radius of the benchmark fan and $\Delta r(z^*)$ is the local deviation from $r_{h,0}$. $z^*=(z-z_{LE})/(z_{TE}-z_{LE})$ is the axial coordinate normalized with the axial length between leading and trailing edge. Six parameters were defined:

- Start and end of the non-cylindrical shape: z_1^*, z_4^*
- Axial position and magnitude of two local extremes: z_2^*, Δr_2, z_3^*, Δr_3

The radius upstream of z_1^* and downstream of z_4^* is unchanged, i.e. $\Delta r(z^* \leq z_1^*)=\Delta r(z^* \geq z_4^*)=0$. The curvature between the four points given is described by cubic functions. The slopes of $r_h^*(z^*)$ at point 1 and 4, i.e. the start and end of the non-cylindrical shape, are required to be 0. Figure 4 shows a schematic of hub curvature and indicates the six parameters.

Optimization loops

All optimization work was done by means of the Nelder-Mead method [13]. The reason for this selection was that this method leads to enhanced solutions after a comparatively low number of runs. The optimization processes were stopped manually when the additional benefit from further runs was not expected to justify further computational cost. The design target in all optimization loops was minimization of losses, i.e. maximization of total-to-total fan efficiency which is defined by

$$\eta_{tt} = \frac{\Delta p_{tt}\dot{V}}{P} \tag{3}$$

Since the Nelder-Mead method is prone to converge to local extremes, the initialization plays an important role. It requires a starting "simplex" with *N+1* edges (= fan designs), *N* being the number of optimization parameters. The parameter variations in the starting simplex must be linearly independent. It was decided to have the values of the benchmark fan in the starting simplex to ensure improvement over the benchmark even if a local optimum is approached. The starting simplex of the hub contour contains a design with reduced radius in the front part of the blade and another design with increased radius in the rear part (#6/7 in Table 2). Since this is anticipation of the expected outcomes, it would have been useful to run the same optimization with a different initialization which was, however, prohibitive due to the immense computational cost.

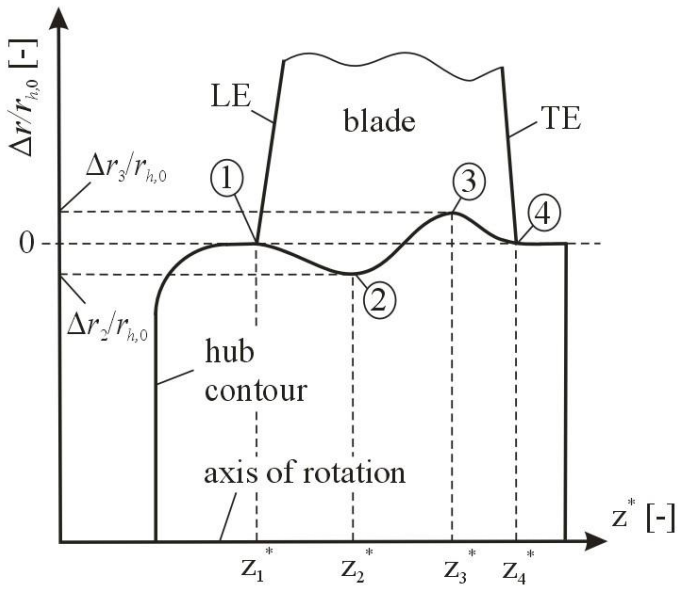

Figure 4: Definition of hub contour parameters.

Table 2: Starting points of the optimization processes.
h=hub, m=midspan, s=shroud

Blade profile							*Hub contour*					
#	$(f/l)_h$	$(f/l)_m$	$(f/l)_s$	$(x_f/l)_h$	$(x_f/)l_m$	$(x_f/l)_s$	z_1^*	z_2^*	z_3^*	z_4^*	$\Delta r_2/r_{h,0}$	$\Delta r_3/r_{h,0}$
1	0.04	0.04	0.04	0.5	0.5	0.5	0	0.3	0.7	1	0	0
2	0.045	0.04	0.04	0.5	0.5	0.5	-0.1	0.3	0.7	1	0	0
3	0.04	0.045	0.04	0.5	0.5	0.5	0	0.35	0.7	1	0	0
4	0.04	0.04	0.045	0.5	0.5	0.5	0	0.3	0.75	1	0	0
5	0.04	0.04	0.04	0.55	0.5	0.5	0	0.3	0.7	1.1	0	0
6	0.04	0.04	0.04	0.5	0.55	0.5	0	0.3	0.7	1	-2	0
7	0.04	0.04	0.04	0.5	0.5	0.55	0	0.3	0.7	1	0	2

CFD simulations

A single rotating computational domain covering the impeller was discretized with the commercial grid generator ANSYS TurboGrid 12.1. All grids are block-structured and contain approx. one million hexahedral elements. The domain extends one fan diameter upstream and two fan diameters downstream of the blade leading and trailing edge, respectively. A general grid interface (GGI) was placed in the tip clearance which amounts to *0.3* % of the rotor diameter. To save computational time, only one blade passage with periodic boundary conditions at the sides was simulated. Further boundary conditions were rotational speed, given mass flow rate (of the design point) at the inlet, ambient pressure at the outlet and no slip at the walls (hub, shroud and blade). The Reynolds-Averaged Navier-Stokes (RANS) equations were solved with ANSYS CFX 12.1. The selected turbulence model was shear stress transport (SST) and the residual target was 10^{-4} MAX. In the post-processing, the pressure was evaluated at planes halfway between the blade edges and inlet/outlet, respectively, to the blade to minimize anticipated errors at spatial averaging. The total pressure

$$p_t = p + \frac{\rho}{2} c^2 \tag{4}$$

was determined by the area-averaged static pressure p and the mass flow-averaged velocity c in a stationary frame.

Experimental set-up

The characteristic curves of the benchmark and optimized fan were measured at the test rig of the University of Siegen according to DIN 24163 [14]. The fan's suction side is connected to the chamber and exhausts into the free atmosphere. The static pressure is measured in the chamber assuming $p_t=p$ due to the very low flow velocity and atmospheric pressure is assumed downstream of the fan due to the free blowing conditions. This means that it is not possible to determine the total-to-total pressure rise because the swirl energy downstream of the fan cannot be measured. An auxiliary fan is installed upstream of the chamber to facilitate higher flow rates. Air density, volume flow, torque and rotational speed are captured as well and the important dimensionless values φ, ψ and η are computed according to the eqs. 1 - 3.

Sound was measured in a semi-anechoic chamber with three microphones by Brüel&Kjær. The microphones were placed at a distance of 1.3 m from the blade leading edge and at angles of -35, 0 and +35° from the rotation axis. The height of the microphones (distance from floor) was exactly that of the rotation axis. A further microphone was placed in the duct downstream of the fan. This configuration allows determining the sound power level L_{W4} in the semi-anechoic chamber as well as the sound power level L_{W5} in the duct (according to DIN ISO 5136 [15]). The sound power level was derived from the measured sound pressure and the consideration of two surface areas:

$$L_W = \bar{L}_p + 10\,lg\left(\frac{A}{A_0}\right) \text{ dB} \tag{5}$$

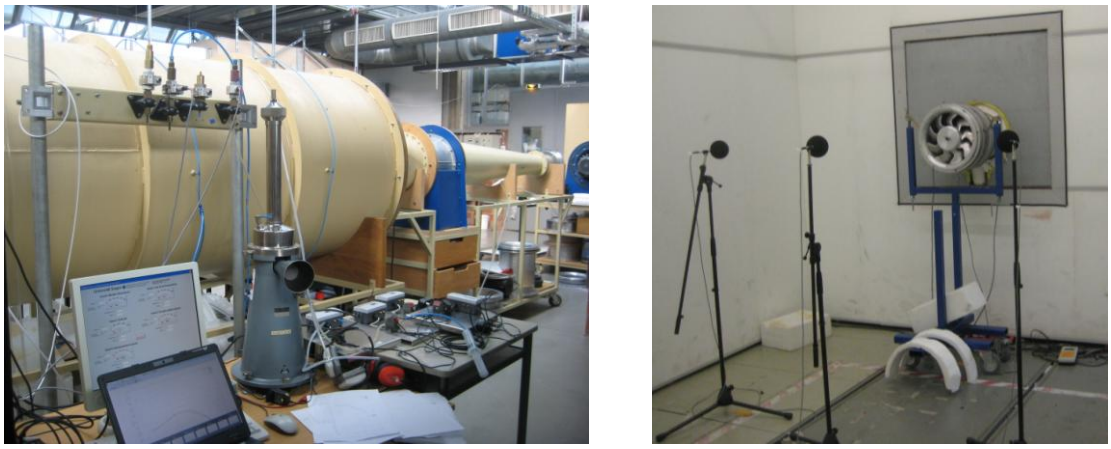

Figure 5: Left: chamber test rig. Right: Set-up for acoustic measurements in semi-anechoic chamber.

where A is the surface area of a hemisphere (L_{W4}) or of the duct cross section (L_{W5}) in which the microphones are placed and A_0=1 m^2 is a reference surface. All measurements were conducted at a rotational speed of 2500 min^{-1}.

RESULTS

Optimized geometry parameters

Table 3 summarizes the optimized design parameters. The optimization yields that regarding the blade profile there is a clear distinction between radial positions near hub/tip and midspan: Near hub and tip f/l is considerably lower and the x_f/l is closer to the trailing edge as compared to the midspan blade sections. In contrast, f/l was increased at midspan and x_f/l was shifted towards the leading edge. The optimized hub has a wavy shape with reduced radius in the front part and increased radius in the rear part of the blade. In total, the new camber distribution leads to reduced averaged lift which means that the chord length of the new profile is longer than before. Figure 6 shows the benchmark and optimized fans. Note the difference in chord length and the modification of the LE/TE curvature.

Validation of the numerical results

The numerical and experimental results are compared in Figure 7. Overall, the characteristic curves show excellent agreement except for a slight tendency to underpredict efficiency in overload and to overpredict pressure rise and efficiency near stall. Nevertheless the validation is considered successful. In the following, comparisons between the two fans will be made using the experimental results as they are more reliable. The CFD results will be used for flow visualizations.

Table 3: Optimized design parameters.

Blade profile			*Hub contour*		
	Benchmark	Optimized		Benchmark	Optimized
$(f/l)_h$	0.04	0.035	z_1^*	-	-0.112
$(f/l)_m$	0.04	0.058	z_2^*	-	0.337
$(f/l)_s$	0.04	0.021	z_3^*	-	0.763
$(x_f/l)_h$	0.5	0.63	z_4^*	-	1.028
$(x_f/l)_m$	0.5	0.21	$\Delta r_2/r_{h,0}$	0	-0.012
$(x_f/l)_s$	0.5	0.51	$\Delta r_3/r_{h,0}$	0	0.015

Figure 6: Left: Benchmark fan. Right: Optimized fan.

Aerodynamic comparison

Figure 8 compares the two designs in terms of total-to-static pressure rise and efficiency as obtained from the experiments. The operating range was increased remarkably. Moreover, there is moderate improvement of ψ_{ts} and η_{ts} at the design point as it was predicted in the optimization process. The intersection with the ϕ-axis (ψ_{ts}= η_{ts}= 0) is equal.

Acoustic comparison

The sound power level was reduced significantly as it can be seen in Figure 9. Regarding sound power on the fans' suction side in the free field (upstream of the fan) the reduction amounts to 3-4 dB over a wide range in φ. For flow rates with $\dot{\varphi} \leq 0.15$ the difference is even greater which results from the delayed stall. The sound power level on the pressure side in the downstream duct was found to be lower accordingly.

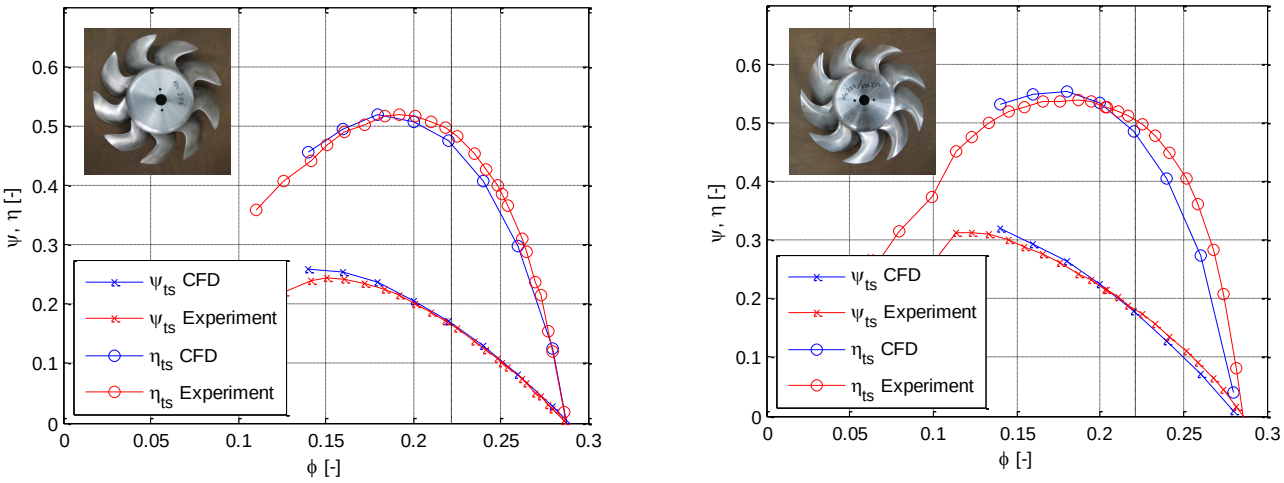

Figure 7: Comparison of numerical and experimental results. Left: benchmark fan. Right: optimized fan.

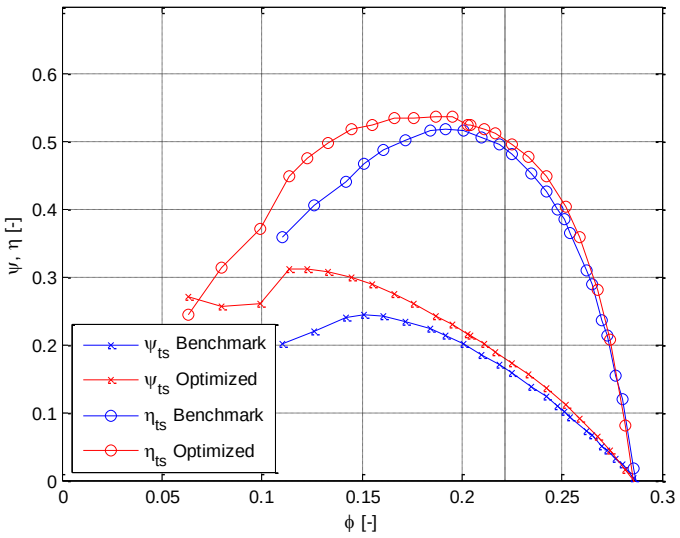

Figure 8: Comparison of measured total-to-static pressure rise and efficiency of both fans.

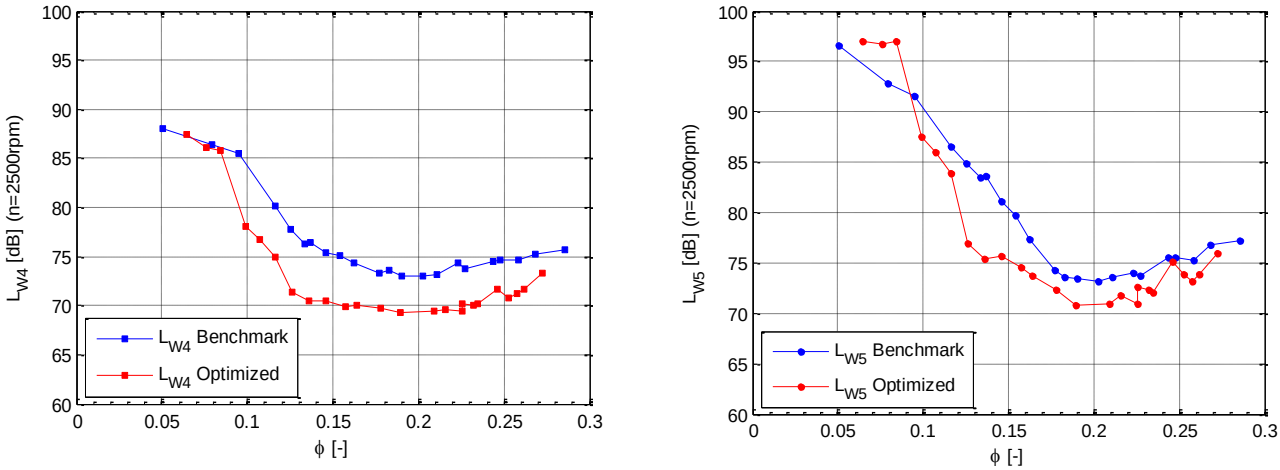

Figure 9: Acoustic comparison of benchmark and optimized fan. Left: sound power level in the room (suction side). Right: sound power level in the downstream duct (pressure side).

Flow visualization

Figure 10 shows a blade passage of the benchmark and optimized fans. The view is towards the blade suction side. The pressure distribution is indicated by a contour plot. Furthermore, the surface streaklines at blade and hub (in the CFX™-jargon: surface streamlines) are shown.

It can be seen that the secondary flows of the boundary layer on the blade suction side have been reduced due to the new blade profile. The new design is less prone to flow separation near the hub which might be ascribed to the reduced camber in this section. In general, the near-hub area is most critical in terms of flow separation because of reduced momentum. By contrast, the increased camber at midspan does not favor flow separation.

The contour plot shows that the new distribution of x_f/l leads to almost isobar pressure distribution in radial direction on the suction side. This contributes to a reduction in radial flow of the boundary layer. The decreased radial flow can be observed in the rear part of the blade in Figure 10.

The hub streamlines also indicate reduction of secondary flow. The cross flow from the pressure side of one blade to the adjacent suction side is still present. However, the separation area is re

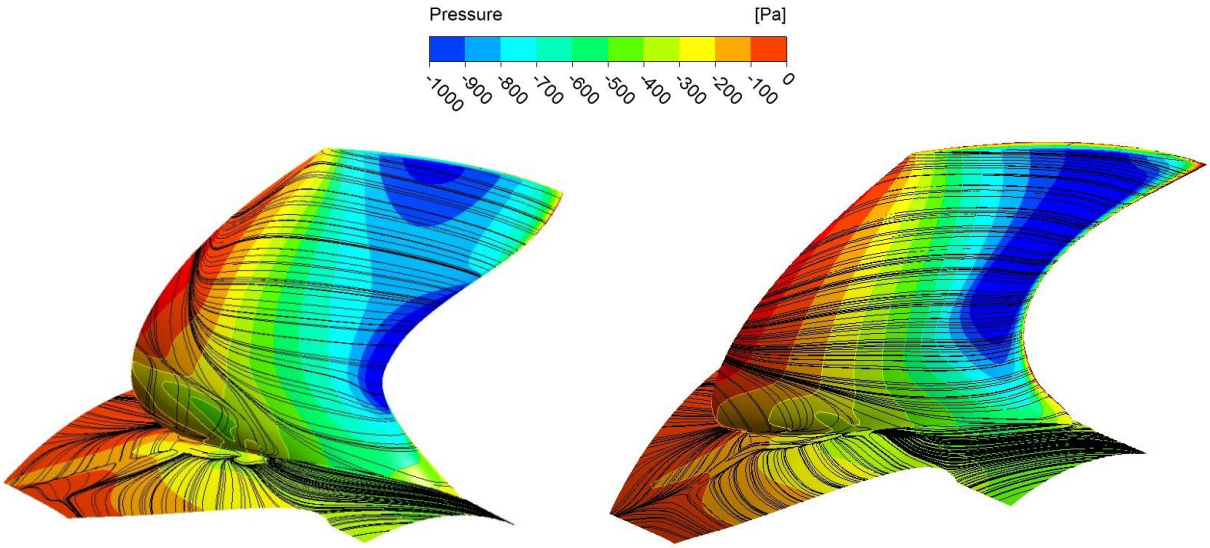

Figure 10: Pressure distribution and surface streamlines from RANS-simulations at benchmark (left) and optimized fan (right). Black lines indicate streamlines. The view is towards the fan suction side.

duced and there is less backflow which has to do with the changed pressure gradients resulting from the trough in the front part (increases pressure) and the hump further downstream (decreases pressure). Note that the modified blade profile also influences the near-hub flow and it is not possible to separate the effect of both modifications in Figure 10.

DISCUSSION AND CONCLUSIONS

A swept benchmark axial fan was optimized aerodynamically and acoustically. Firstly, the magnitude and position of maximum camber of the utilized NACA profile were varied along the blade span. Secondly, a simple kind of axisymmetric hub contouring was applied to address losses linked with the near-wall pressure gradient. Geometrical parameters were defined and the aerodynamic optimum was approached by numerous runs of RANS simulations and a Nelder-Mead optimization method. As target function the total-to-total efficiency at the design point was selected. An important constraint in the optimization cycle was constant chord length in spanwise direction ensuring equal sweep at leading and trailing edge throughout the optimization; this means turning away from predefined spanwise aerodynamic load distributions.

It became evident that both, a wave shaped hub contour along the blade channel and a new distribution of magnitude and position of maximum camber of the utilized NACA profile can manipulate unfavorable pressure gradients and hence reduce near wall secondary flow losses. The angle of attack was not optimized but is still selected according to the 2D airfoil polars. Eventually, the characteristic curves of the optimized design was predicted via RANS and experimentally validated. The test results showed good agreement with the simulations. The aerodynamic benefit of the new design was a moderate increase in efficiency near design point but a remarkable extension of operating range. Moreover, acoustic investigations showed a considerable reduction in sound power over the complete operating range.

The most important limitation of this work is that many geometrical modifications were treated simultaneously such that the effects of the individual modification are difficult to separate. Especially regarding the sound emission it is not possible to ascribe the reduction to either the new sweep strategy or to the reduction of secondary flows. Furthermore, only integral values (ψ, η) could be validated experimentally while flow details (such as secondary flows) were only treated numerically. Given these limitations it is concluded that further experiments with intermediate designs (only new sweep, sweep + profile) would be useful. Furthermore, flow details should be examined as

well. Regarding the CFD simulations, transient simulations would provide more details of the secondary flows and also allow for detection of noise sources. The problem that the optimization processes might have converged to local extremes can be solved by new runs with different initialization or the application of other optimization methods. Similar investigations at fans with different design point and different sweep are suggested to check the transferability of the results. Furthermore, best practice design recommendations in terms of blade profile and hub geometry that are based on this work would be helpful for fan designers since the procedure described is prohibitively time consuming in most cases.

ACKNOWLEDGEMENT

Parts of this investigation were funded by the European Commission within the project ECO-QUEST (grant agreement number 233541) of the Seventh Framework Programme.

BIBLIOGRAPHY

[1] Beiler, M. G., Carolus T. H. - *Computation and Measurement of the Flow in Axial Flow Fans With Skewed Blades*. Journal of Turbomachinery 121, pp. 59-66, **1999**

[2] T. Wright, W. E. Simmons - *Blade Sweep for Low-Speed Axial Fans*. Journal of Turbomachinery 112, pp. 151-158, **1990**

[3] T. Carolus, M. Beiler - *Skewed Blades in low Pressure Fans: A Survey of Noise Reduction Mechanisms*. AIAA-97-1591, pp. 47-53, **1997**

[4] E. J. Kerschen - *Noise Generation by a Finite Span Swept Airfoil*. AIAA-83-0768, **1983**

[5] J. E. Ffowcs, L. H. Hall - *Aerodynamic Noise Generation by Turbulent Flow in the Vicinity of a Scattering Half Plane*. Journal of Fluid Mechanics 40, pp. 657-670, **1970**

[6] T. Carolus - *Ventilatoren - Aerodynamischer Entwurf, Schallvorhersage, Konstruktion (2. Auflage)*. Wiesbaden: B. G. Teubner / GWV Fachverlage GmbH, **2009**

[7] I. H. Abbot, A. E. von Doenhoff - Theory of Wing Sections. New York: Dover Publications Inc., **1959**

[8] M. Zangeneh - *A Compressible Three-Dimensional Design Method for Radial and Mixed Flow Turbomachinery Blades.* Journal of Numerical Methods in Fluids 13, pp. 599-624, **1991**

[9] K. Takeishi et al. - *An Experimental Study of Heat Transfer and Film Cooling on Low Aspect Ratio Turbine Nozzles.* Journal of Turbomachinery 112, pp. 488-496, **1990**

[10] N. W. Harvey, M. G. Rose - *Bladed Ducting for Turbomachinery*. United States Patent No. US 6,283,713 B1, **2001**

[11] G. Kröger et al. - *Theory and Application of Axisymmetric Endwall Contouring for Compressors*. Proceedings of ASME Turbo Expo GT2011-45624, **2011**

[12] D. Thévenin, G. Janiga - *Optimization and Computational Fluid Dynamics*. Heidelberg: Springer Verlag GmbH, **2008**

[13] J. A. Nelder, R. Mead - *A Simplex Method for Function Minimization*. Computer Journal 7, pp. 308-313, **1965**

[14] DIN 24163 - *Fans; performance testing, standard characteristics.* Deutsche Norm, Berlin, **1985**

[15] DIN ISO 5136 - *Bestimmung der von Ventilatoren und anderen Strömungsmaschinen in Kanäle abgestrahlten Schalleistung*, Deutsche Norm, Berlin, **2000**